Cement 14 (2023) 100085

Contents lists available at ScienceDirect

Cement

journal homepage: www.sciencedirect.com/journal/cement

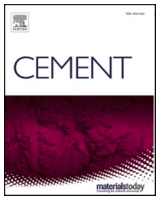

Early age reaction of slag in composite cement: Impact of sulphates and calcite

Sam Adu-Amankwah [a,b,*], Leon Black [b], Liu Xianfeng [c], Pengkun Hou [d], Maciej Zajac [e]

[a] Department of Civil Engineering, Aston University Birmingham, Aston St, United Kingdom of Great Britain and Northern Ireland, B4 7ET, United Kingdom
[b] School of Civil Engineering, University of Leeds, Woodhouse Ln., Leeds LS2 9JT, United Kingdom of Great Britain and Northern Ireland, United Kingdom
[c] Department of Road and Railway Engineering, Southwest Jiaotong University, Chengdu, Sichuan, China
[d] Department of Materials Science & Engineering, University of Jinan, Shandong, China
[e] Global R&D Heidelberg Materials AG, Oberklamweg 2-4, 69181, Leimen, Germany

ARTICLE INFO

Keywords:
Sulphates
GGBS/slag
Hydration
Microstructure
Low carbon cement, Limestone ternary cement

ABSTRACT

Ground granulated blast furnace slag (GGBS) is an important supplementary cementitious material (SCM) for producing low carbon and durable concrete. There are however questions around the early age reactivity of GGBS and the factors that influence this. To elucidate the fundamental mechanisms controlling the early age reactivity and particularly the influence of anionic species, simplified systems comprising GGBS and calcium hydroxide were examined in the presence of limestone, anhydrite, or both at 4:1 SCM-to-activator ratio. Limestone and GGBS were considered as SCMs, but calcium hydroxide and anhydrite were considered as activators. Multiple techniques, including isothermal calorimetry, thermogravimetry, X-ray diffraction, electron microscopy, mass balance calculation and mercury intrusion porosimetry were used to study hydration and microstructure. The results show that GGBS hydration commences immediately in the alkaline media provided by calcium hydroxide. Sulphates and limestone influence hydration through reactions with aluminates to form ettringite and carboaluminates, but prevalence of macro-capillary pores in sulphate containing binders sustains diffusion-controlled hydration. Consequently, optimization of the alumina to sulphate and carbonate ratios is essential for exploiting the pore solution and space filling effects in composite cements.

Introduction

The reactivity of supplementary cementitious materials e.g., GGBS is an important step for optimizing their contribution, as well as predicting the evolution of phase assemblages and performance of low carbon cements. Previous studies [1–3] have reported extensively on the physical and chemical factors which influence reactivity of GGBS-based composite cements. In these cements, grinding the clinker or GGBS finer helps to improve early-age reactions by increasing the surface area available for hydration [4,5]. However, in the long-term the clinker fineness seems to have a limited impact [6] whilst GGBS is also harder to grind and hence, the associated benefits do not always justify finer grinding. Consequently, the mechanical route to improving the reactivity of slag is constrained.

The reactivity of GGBS strongly depends on its chemical composition, glassy phase content and conditions of the reacting medium e.g., pH, temperature etc. Parametric studies on GGBS/calcium hydroxide with or without sulphate systems have shown enhanced GGBS reactivity at higher calcium hydroxide (CH) content and further reactivity with sulphate [7,8]. Several authors have also studied the impact of chemical compositions on the reactivity of slag [9–15]. This is enhanced with increasing magnesium oxide [16] and alumina oxide [14,17,18] contents. Meanwhile, in high alumina slag cements, the alumina concentration in the pore solution is increased, which is incorporated into the calcium silicate hydrate (C-S-H) and hydrotalcite [14]. However, in the presence of secondary anionic species such as sulphates and calcite, alumina containing phase assemblages including ettringite and carboaluminates are formed instead [10,19], reducing the alumina incorporation into the C-S-H. Some studies [12,20] have shown improved silicate dissolution, including slag, at lower alumina levels in the pore solution, but recent studies have also highlighted the important role of calcium activity [13,21]. Therefore, the drivers for the advantageous

* Corresponding author at: Department of Civil Engineering, Aston University Birmingham, Aston St, United Kingdom of Great Britain and Northern Ireland B4 7ET, United Kingdom.
E-mail address: s.adu-amankwah@aston.ac.uk (S. Adu-Amankwah).

https://doi.org/10.1016/j.cement.2023.100085
Received 28 March 2023; Received in revised form 31 July 2023; Accepted 3 September 2023
Available online 7 September 2023

effects of alumina and magnesium on slag dissolution seem to arise from the uptake of alumina into hydrates [19] and the distribution of hydrates [10,22], which brings into question the role of anionic species in the pore solution.

GGBS in composite cements generally hydrates at a much slower rate compared to cement clinker [23,24]. At early stages of hydration, slag exerts a filler effect by providing nucleation sites and increasing the effective water available for clinker hydration [3,25]. Not only does the accelerated clinker hydration lead to formation of more calcium hydroxide and C-S-H, but it also increases the dominance of alkalis in the pore solution. This raises the pH and thus provides the alkaline medium necessary for slag hydration. It may therefore seem that the limiting step for slag hydration is the availability of hydroxyl ions near the reacting surface. This hypothesis seems valid as long as kinetics are controlled by the GGBS dissolution rate. However, at longer hydration times, where kinetics become transport-controlled [21,26], the nature of hydrates surrounding the slag particles may play a critical role in controlling reactivity.

Several mechanisms regarding the role of aluminosilicate dissolution have been postulated elsewhere [20,27–29]. Oelkers et al. [28] and other authors [29,30] have suggested a surface desorption mechanism where an alumina deficiency weakens the alumino-silicate structure, promoting silicate dissolution. An interface-limited mechanism has also been suggested elsewhere [27]. Both mechanisms very much depend on the concentration of the dissolved species as well as the nature and distribution of the reaction products. For example, Berg and Banwart [30] found direct correlation between carbonate ion concentration and the rate of aluminium release. A similar effect for sulphate was observed in our previous study [31], where the calcium and sulphate concentrations in the pore solution decreased sharply after 24 h while that of aluminium increased. However, the reaction products of carbonates and sulphates differ in aluminium uptake capacity [32,33] and densities [34] and can be modified by anions in the pore solution [12,35–38]. This is particularly true of the AFm phases, precipitation of which is required to maintain ionic balance in the pore solution, and consequently to dissolution of constituents. The objective of the present paper is to clarify the mechanism through which anionic species in the pore solution of composite cements including carbonates, sulphates or their combination influence the reaction of GGBS.

Experimental details

Materials

The binders investigated were prepared from commercial grade GGBS (supplied by Heidelberg Materials) and calcium hydroxide powder (purchased from Fischer Scientific) mixed with either limestone, natural anhydrite, or both. The chemical compositions and specific surface areas of the materials, as determined by x-ray fluorescence (XRF) and Blaine measurements respectively, are shown in Table 1. The mineralogical composition of the materials is shown in Table 2. The particle size distributions of the constituent materials, measured by laser granulometry, are shown in Fig. 1 and the mix proportions are detailed in Table 3. Finally, DTA curves confirming purity of limestone, calcium hydroxide and anhydrite used in the present study alongside with devitrification of slag at high temperatures, indicative of glassy phase transitions are shown in Fig. 2. The soluble anhydrite endotherm at 130 °C, γ-$CaSO_4$ is noteworthy and this will be used to follow its consumption as it transitions into β-$CaSO_4$ with increasing temperature [39]. In designing the mixes, limestone partly substituted for slag while anhydrite partly replaced calcium hydroxide as an activator. Consequently, a constant activator (i.e., calcium hydroxide and anhydrite) to SCM ratio (i.e., GGBS, and limestone where applicable) was maintained at 1:4. This was chosen to mimic early age composition in blended cements with up to 50% clinker replacement [40], being consistent with those reported elsewhere e.g., [41,42] but lower than for the R3 test [43].

Methods

The constituent materials were weighed and homogenized in a laboratory ball mill for at least 3 h using polymer balls to prevent further grinding. Paste samples were prepared at 0.5 water/solid (w/s) ratio, corresponding to typical water/binder ratios for cement paste, and mixing performed on a vortex mixer for 2 min. Isothermal conduction calorimetry, x-ray powder diffraction (XRD), thermogravimetric analysis (TGA), SEM/EDX and MIP were combined to investigate kinetics, phase assemblages and the pore structure.

Isothermal calorimetry was conducted on 9 g paste samples and the heat of reaction was continuously measured for 7 days at 20 °C using an 8-channel TAM Air calorimeter. Reference channels were filled with ampoules containing 6 g of quartz mixed with 3 g of deionized water.

Samples for microanalysis were cast into 10 ml plastic vials, sealed and rotated for the first 24 h to prevent bleeding. Whilst still under sealed conditions, the samples were stored in a water bath until testing. XRD scans were performed on freshly ground samples aged 0.5 to 28 days without hydration stopping after covering with Kapton film to prevent drying and carbonation during the data acquisition. For TGA and MIP, the specimens were hydration stopped by the double solvent change technique [35]. The solvent exchange regime involved grinding in IPA for 20 min and filtering off the IPA under gravity in a glovebox which was kept free of CO_2 by purging with nitrogen gas. The residue was rinsed in diethyl ether before drying at 40 °C on a pre-heated glass plate for 20 min. Following hydration stopping, samples were stored in mini-grip bags in a glovebox until analysis.

XRD data were acquired on a PANalytical MPD Pro-using a CuKα anode operating at 40 kV and 40 mA, over a range of 5–80°2θ. The step size was 0.334°2θ and 0.06 s per step, using the scanning X'Celerator detector. Automatic incident divergence and fixed anti-scatter slits were used together with a 10 mm incident beam mask. The continuous scan mode was adopted for all data acquisition. Following, the data was analysed on TOPAS Academic software v4.2. A first order Chebyshev polynomial background function was adopted for modelling and calibrating the GGBS PONKCS phase. The fundamental parameter approach was used to model the slag phase. Details of the calibration of the slag phase and validation of the model are described elsewhere [40]. This PONKCS phase was subsequently implemented in the Rietveld refinement to determine the residual slag content as well as crystalline hydration products.

TGA was carried out under nitrogen on 16–18 mg of additionally ground powder sample using a Stanton 780 Series Analyser. The heating range was 20–1000 °C at a rate of 20 °C/min. The bound water contents were computed as the percentage weight loss between 50 and 400 °C according to Eq. (1).

Table 1
Oxide composition of raw materials (% weight).

Composition	SiO_2	Al_2O_3	MgO	CaO	K_2O	Fe_2O_3	SO_3	LOI	Blaine (kg/m^2)
Slag [S]	34.87	11.62	5.82	41.82	0.47	0.45	3.13	1.13	454
Limestone [L]	2.00	0.08	0.64	53.13	0.10	0.32	0.07	42.3	328
Anhydrite [s]	2.04	0.60	1.45	38.32	0.16	0.23	52.24	3.68	472

Table 2
Mineralogical composition of supplementary materials (% weight).

Material/Phase	Calcite	Portlandite	Quartz	Anhydrite	Amorphous	Others
Slag (S)	2.4		0.1	–	97.5	
Calcium hydroxide (P)	1.2	98.2				0.6
Limestone (L)	99.6		0.4	–	–	
Anhydrite (s)	–		1.02	98.98	–	

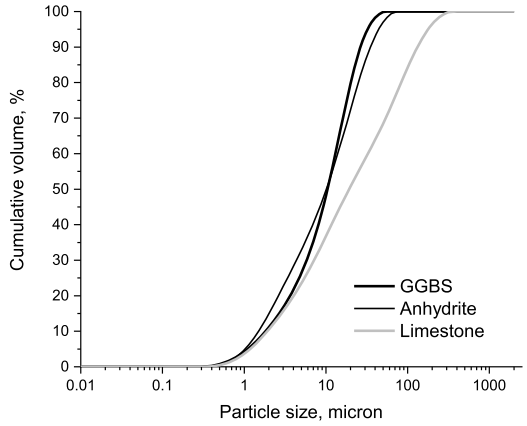

Fig. 1. Particle size distribution of constituent materials.

$$W_n = \frac{M_{50\ ^oC} - M_{400\ ^oC}}{M_{400\ ^oC}} * 100 \quad (1)$$

where, W_n is bound water content, $M_{50\ ^oC}$ is ignited weight at 50 °C, M_{400^oC} is ignited weight at 400 °C.

The range was chosen to exclude the water contained in calcium hydroxide, which was a reactant in this case. Calcium hydroxide decomposition commenced at 400 °C in all the investigated mixes hence an upper limit of 400 °C for the bound water calculations. This assures internal consistency of the systems investigated. Similarly, calcium hydroxide consumption was calculated from the residual content using the tangent method in the 400 – 500 °C range.

Samples for SEM were 2 mm thick discs, which were hydration stopped by freeze-drying following the protocol in [14]. This comprised immersion of specimens in liquid nitrogen before placing in the freeze-dryer until constant mass. After hydration stopping, samples were resin impregnated and polished down to 0.25 μm using a combination of silicon carbide abrasive cloths with diamond paste. Images were acquired in backscattered electron mode using a Zeiss EVO MA15 equipped with an 80 mm detector. The instrument was operated at 15 kV accelerating voltage. EDX point analysis was also performed to determine composition of the hydrated matrix.

Ternary phase diagram calculations were used to predict stable phase assemblages and their contents after 28d hydration as means of validating the QXRD/ PONKCS results. The methodology according to Herfort and Lothenbach [44] was employed, taking into account the bulk composition of constituent materials based on XRF and degree of reaction after 28 days from QXRD/PONKCS. This was particularly important for evaluating the poorly crystalline assemblages that may not be accurately quantified from Rietveld refinement.

MIP measurements were performed on 1 – 2 mm thick crushed hydrated cement samples using a Micromeritics AutoPore IV 9500 with a maximum pressure of 228 MPa. The principle of MIP is based on the Washburn's Eq. (2), which expresses the applied pressure, Pc, for mercury intrusion into a cylindrical tube as a function of the entrance pore diameter, d.

$$P_c = \frac{-4\gamma Cos\theta}{d} \quad (2)$$

where θ is the contact angle between the liquid mercury and the solid surface (140° is used) and γ is the mercury surface tension (0.484 N/m). The pore structure was characterised in terms of the pore distribution and the total pore volume.

Results

Kinetics of hydration

The heat flow normalised to the GGBS content is shown in Fig. 3a. There is the immediate onset of GGBS reaction in the alkaline medium. The heat profiles showed an induction, acceleration, deceleration, and steady state reactions similar to clinker-based systems. The heat flow curve is characterised by the main reaction peak and a shoulder, attributable to slag dissolution and precipitation of hydrates respectively. Onset of the acceleration phase was faster in the mixes containing limestone (see the insert in Fig. 3a). The slope of the acceleration stage was similar in all mixes, but slightly offset in the mix S-P-20 L and to a smaller extent the S-P-5s-5 L. In the presence of limestone without sulphates, a slight hump was noticed after ~2 h and the slope was less steep

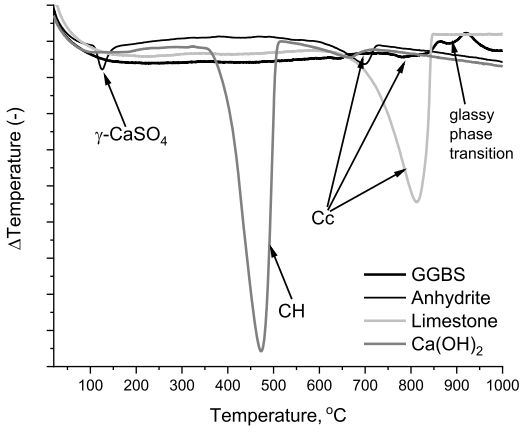

Fig. 2. DTA trace of slag, anhydrite, and limestone.
CH: calcium hydroxide; Cc: calcite.

Table 3
Composition of mixes investigated (%).

Mix designation	GGBS	Calcium hydroxide	Limestone	Anhydrite	Water	Volume fraction of slag (%)	Calcium hydroxide/ GGBS
S-P	80	20	–	–	50	53.3	0.25
S-P-5s	80	15	–	5	50	53.3	0.19
S-P-20L	60	20	20	–	50	40	0.33
S-P-5L-5s	75	15	5	5	50	50	0.2

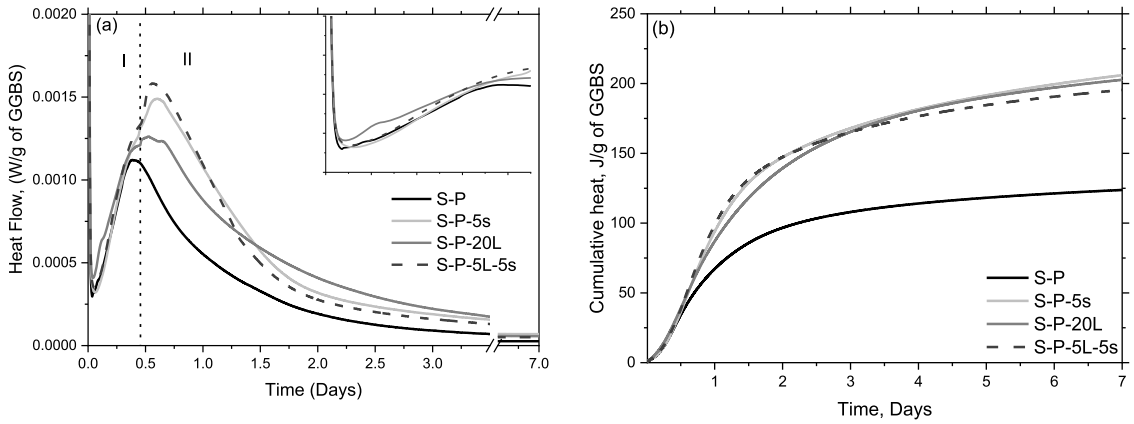

Fig. 3. Heat of reaction of mixes showing the effect of anionic species on reaction of GGBS (a) heat flow, insert shows the onset of acceleration phase of hydration; and (b) cumulative heat as measured by isothermal calorimetry. S: GGBS, P: Calcium hydroxide, L: limestone, s: anhydrite.

compared to only sulphate or limestone with sulphate. However, occurrence of the main reaction peak was less sensitive to the anionic species except in its intensity. The intensity was higher in the mixes containing limestone and sulphates compared to the control mix (S-P). The effect of combined carbonate and sulphate therefore appears to be cumulative.

Anhydrite and limestone modified the shoulder to the main reaction peak differently as did their combination. In the S-P mix, the shoulder was not discernible from the main peak whilst the overall reaction heat was much lower (Fig. 3b). Meanwhile, the main peak occurred around the same time (~18 h) in the mixes containing anhydrite, limestone, or both, but the cumulative heat profile was sensitive to the additions. The sulphate-containing mixes showed higher intensity, plausibly linked to the enhanced slag dissolution. The deceleration slope after the shoulder was steeper in the sulphate-containing mixes, suggestive of solid calcium sulphate depletion in the pore solution and rapid precipitation of ettringite [36,45]. The results reveal accelerated depletion of sulphates and precipitation of ettringite in the presence of limestone. It is noteworthy that, despite having a lower heat intensity, reaction of the mix containing only limestone evolved comparable heat to the other sulphates mixes with or without limestone after ~1.5 days, leading to an overall higher cumulative heat than those containing sulphates (Fig. 3b) by 7 days.

XRD signals showing kinetics of calcium hydroxide, sulphate and limestone consumption up to 28 days of hydration are shown in Fig. 4. Here only reflections for the phases mentioned above have been shown for clarity. From the main reflections at ~18.1 and 34.2 °2θ, calcium hydroxide was still present in all mixes after 28 days but its consumption was more gradual in the mixes S-P and S-P-20 L compared to the mixes that contained sulphates with or without limestone. Meanwhile, crystalline anhydrite (25.5 °2θ) was depleted by 1d in the mix that contained limestone and sulphate whilst a noticeable reflection was still present in the mix without limestone (S-P-5s) even after 2 days. These observations are consistent with the calorimetry data, which revealed faster deceleration once anhydrite was depleted.

The derivative thermogravimetric (DTG) plots in Fig. 5a and 5b show water loss associated with the C-A-S-H phase in all mixes, plus ettringite in the sulphate-containing mixes. The mass loss in this region (20 – 150 °C) was comparable in the mixes S-P and S-P-20L, being approximately 2.3 and 2.17% respectively, but exceeded 5% in the sulphate-containing mixes, and increased slightly further when limestone was also present. Meanwhile, from the thermal transitions of anhydrite, Fig. 5a also confirms its persistence in the mix that contained 5% anhydrite, but depletion in the composite anhydrite and limestone mix after 1d. These observations imply that the synergy between sulphates and calcium carbonate did not only accelerate consumption of sulphates but precipitated phase assemblages too.

The endotherms associated with calcium hydroxide and calcite decreased with time (Fig. 5a and 5b), indicative of continuing reaction which led to increased contents of C-A-S-H, ettringite, carboaluminates and hydrotalcite. Limestone appeared to have had no measurable influence on the C-A-S-H and ettringite endotherms in the sulphate-containing systems. Similarly, in the mixes without added anhydrite, limestone did not influence the C-A-S-H and ettringite endotherms

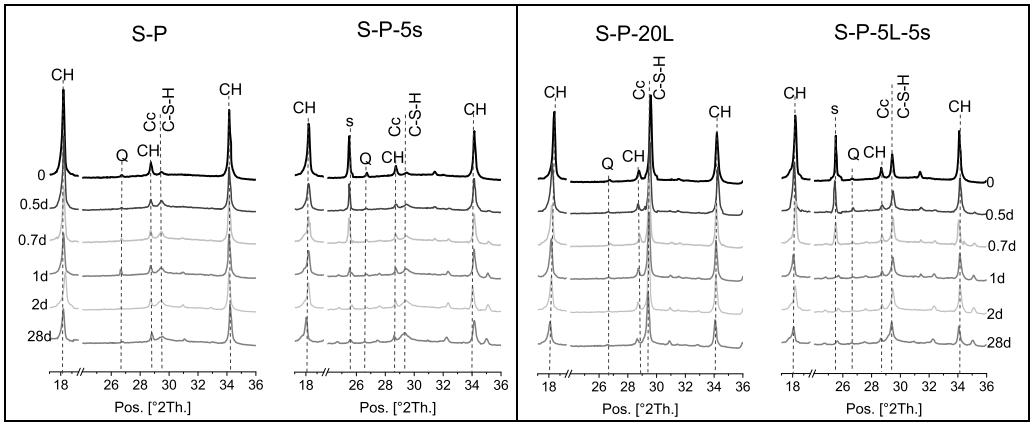

Fig. 4. X-ray diffraction patterns showing consumption of calcium hydroxide (CH), limestone (Cc) and anhydrite(s) in the investigated mixes up for the first 2 days of reaction.
Note: Q is trace of quartz in the GGBS.

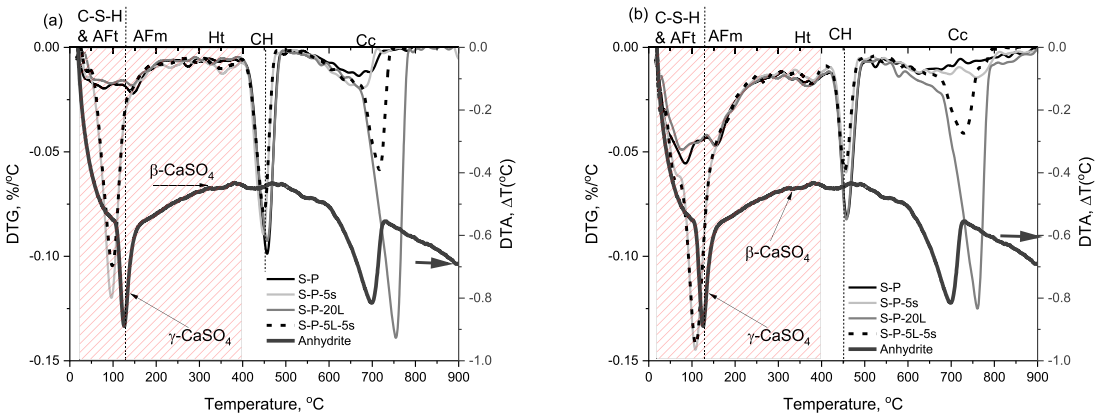

Fig. 5. Thermal analysis of investigated mixes plotted in terms of DTG curves after reacting for (a) 1 day and (b) 28 days alongside DTA trace of the as-received anhydrite.
Aft: ettringite; AFm denotes carboaluminates and monosulphoaluminate; Ht: hydrotalcite.

significantly; instead, an AFm phase was formed with or without limestone. The formation of such a phase in mix S-P could be due to traces of calcite in the GGBS and or calcium hydroxide as can be seen from the DTA in Fig. 2 or formation of sulphate-bearing AFm in the 5% sulphate mix (i.e., S-P-5s). In the mix S-P, without limestone and sulphates, a hydrotalcite phase evident from an endotherm at about 350 °C was observed from 2 days onwards. The signal was weaker in the mixes containing sulphates and limestone after 1 day, but it was conspicuous in all mixes after 28 days.

Though the added limestone (in S-P vs. S-P-20L and S-P-5s vs. S-P-5L-5s) did not lead to new DTG identifiable phase assemblages, one must recognize that it replaced 20 and 5% of GGBS respectively. Therefore, its effect on the increased volume of phase assemblages is noteworthy and consistent with the cumulative heat in Fig. 2.

Microstructure evolution

Phase assemblages and distribution

The stable phase assemblages predicted from mass balance calculations are shown in Fig. 6. Note that the reactants including GGBS, limestone and free water have been excluded from the plot for clarity. Hydrotalcite and C-A-S-H are predicted in all mixes, whilst hemi- or monocarboaluminates formed from the trace calcite in the slag and from the additionally added limestone. The additional limestone however, stabilized mono- over hemicarboaluminate, but the continual presence of sulphates hindered calcite reaction and hence carboaluminate formation. Meanwhile, ettringite only formed in the presence of anhydrite,

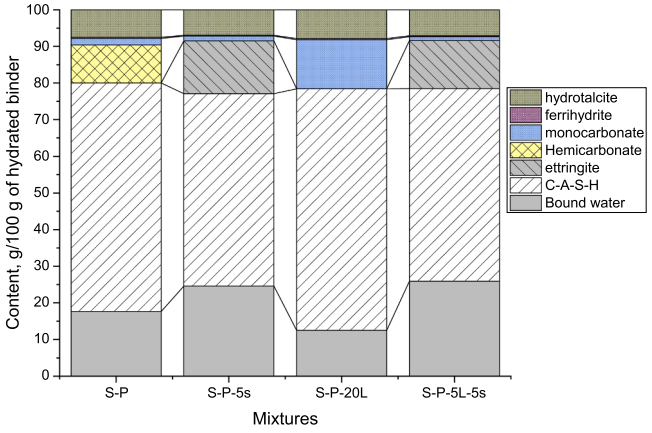

Fig. 6. Predicted stable phase assemblages formed in the investigated compositions from mass balance calculations.

which suggests that sulphides in the GGBS did not contribute to ettringite formation in these systems. Fig. 5 confirmed the predicted phase assemblages and their variation as a function of the anionic species present in the matrix.

The above predicted phase assemblages and their distribution in the reacting matrix characterised the microstructures. Illustrative backscattered SEM images of the binders recorded after 1 and 28 days of reaction are shown in Fig. 7 (a–h).

After 1-day, porous microstructures comprising unreacted slag and calcium hydroxide, together with some hydration products, were observed in all mixes. The nature of the reaction products and their distribution however depended strongly on the mix composition. In the mix containing slag and calcium hydroxide only (S-P in Fig. 7 (a and b), C-A-S-H was observed to precipitate around the reacting GGBS grains. Progressive hydration increased the size of the hydrates such that after 28 days, a thick layer can be noticed around individual GGBS particles, with pockets of pores between adjacent rims.

In the mix, S-P-5s where 5% anhydrite was added, ettringite was the dominant product after 1 day. The crystals however precipitated in the voids away from the GGBS particles, as can be seen from Fig. 7 (c and d). As hydration progressed, the reaction products filled the spaces around the needle-like ettringite. The rims around GGBS particles, as observed in the mix S-P, were not very clear in the presence of sulphates; instead, intermixing of C-A-S-H and ettringite was observed. In the presence of limestone, Fig. 7 (e and f) show hydrates in the spaces between the GGBS particles rather than around them. By 28 days, a much more compact and less porous microstructure was noticed around the limestone particles. Rims around the GGBS particles were not as distinct as observed in the mix S-P. When limestone and anhydrite were present, see Fig. 7 (g and h), the microstructure after 1 day was dominated by ettringite.

Here ettringite appeared to form away from the GGBS particles, as was the case in the mix S-P-5s. Moreover, the capillary pores after 1 day (as noticeable from Fig. 7g), was much lower compared to the mixes with either anhydrite or limestone only (i.e., Fig. 7a and 7c). By 28 days, the microstructure was a mixture of ettringite, C-A-S-H and AFm phases. Their distribution had attributes of the S-P-5 s and S-P-20 L microstructures, in terms of the needle-like features and denser hydrates. Additionally, a dark rim could be seen around the limestone particle, as shown in Fig. 7h, suggestive of calcite consumption. The consumption of calcium hydroxide and calcite with the formation of the reaction products is consistent with the calorimetry and XRD data.

Calcium aluminosilicate hydrates and ettringite identified in Fig. 5 were not the only hydrates, carboaluminates and hydrotalcite also formed. Their evolution as determined from XRD is shown in Fig. 8. Ettringite, hemi-carboaluminates and hydrotalcite were observed as the main crystalline reaction products with their contents increasing with

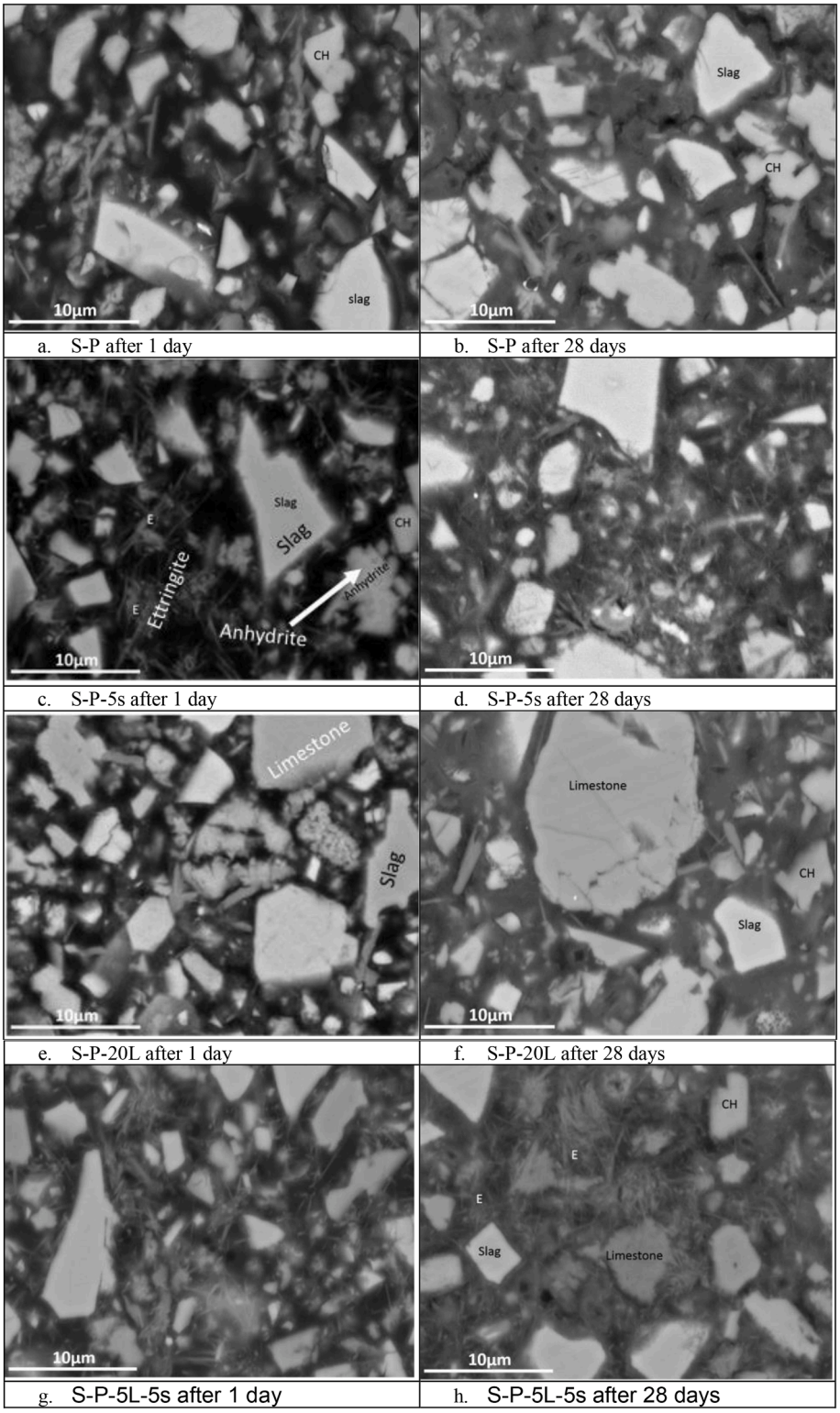

Fig. 7. Nature and distribution of phase assemblages as determined from back scattered SEM. Note: Images were taken at 4000x magnification, resolution 2048 × 1536 pixels and identified features are marked on the micrograph.

hydration time as calcium hydroxide was consumed. After 12 h, an ettringite reflection was already identified in the sulphate-containing mixes (S-P-5 s and S-P-5L-5s), but hemi-carboaluminate was identified in the mixes without added sulphate (S-P and S-P-20L). In the blend with neither added anhydrite nor limestone, hemi-carboaluminate peaks were detected due to the small amount of calcite in the GGBS. However, sulphides (present in 3.13% SO_3) in the anhydrous GGBS did not oxidise and react to form ettringite. Instead, a weak reflection of hydrotalcite was noticed alongside carboaluminates from very early age. More hemi-carboaluminates formed in the blend containing additional limestone (S-P-20L) compared to the mix without added limestone (S-P). Meanwhile, in the blend containing both anhydrite and limestone, traces of anhydrite persisted up to 1 day (Fig. 4) after which weak reflections of hemi-carboaluminate and hydrotalcite were noticed. Comparison with the

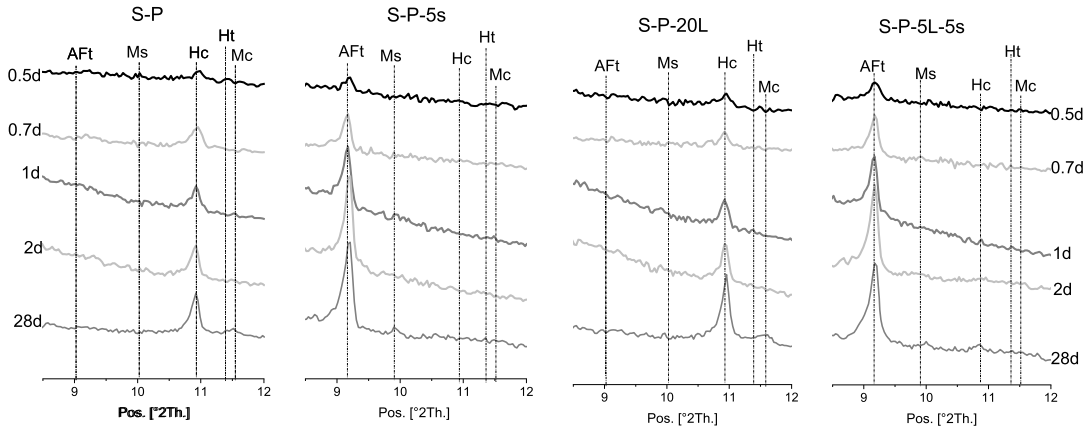

Fig. 8. XRD plots of the investigated mixes showing the evolution of ettringite, carboaluminates/monosulfoaluminate and hydrotalcite.
Note: In the S-P and S-P-5 s mixes, the Mc line is for consistency and similarly the Ms in the S-P-20 L sample, rather than showing the presence thereof.

mix that contained only limestone suggests retarded calcite dissolution in the presence of anhydrite, but without limestone, monosulfoaluminate formed upon anhydrite depletion. Monosulfoaluminate precipitation in the absence of limestone has been reported elsewhere [32,46], but the impact on crystalline hydrotalcite is reported here for the first time. Hydrotalcite was not observed in the sulphate-containing blends over the investigated time range. It has been shown elsewhere, that calcium hydroxide consumption during the pozzolanic reaction could limit hydrotalcite formation [47]. In the results reported here, however, excess calcium hydroxide was present whilst aluminium was released upon GGBS hydration. Therefore, neither calcium hydroxide nor aluminium availability could be considered a limiting factor in hydrotalcite formation, but sulphate in the pore solution may be. This may arise from competitive adsorption between sulphates and carbonates or loss of crystallinity of the hydrotalcite phase in the presence of sulphates.

Bound water content

The bound water content is indicative of the degree of reaction. In this study, the mixes contained calcium hydroxide as a reactant and hence, the bound water content was taken as the ignited weight loss between 50 °C and 400 °C. This range was chosen based on Fig. 5, so that water contained in calcium hydroxide was excluded from the bound water. Consequently, the results presented in Fig. 9 may not be directly comparable to composite cements where calcium hydroxide is a reaction product. The presence of sulphates and limestone increased bound water content per unit GGBS. However, the impact of limestone was small at the early age but became greater over time whilst the combined effect of sulphates and limestone resulted in consistently higher bound water contents than those obtained from the addition of an individual component.

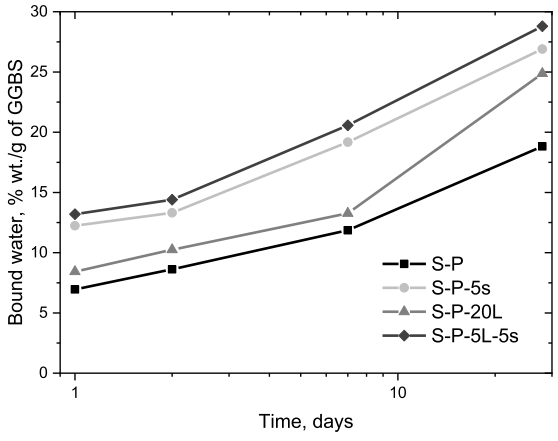

Fig. 9. Effect of limestone and sulphates on the bound water content in calcium hydroxide activated binder, measured by TGA and normalized to the GGBS content.

The hydrates formed in the four systems (Figs. 5 and 7) explain the respective bound water contents. C-[A]-S-H, carboaluminate and hydrotalcite were the dominant reaction products following GGBS hydration in the absence of sulphate. However, in the sulphate-containing mixes, ettringite was formed in addition to C-[A]-S-H and hydrotalcite. Ettringite has an intrinsically higher bound water content than C-S-H and carboaluminates [32,48], and than hydrotalcite [49]. This explains the higher bound water content in the sulphate-containing blends.

Discussion

In composite cements, GGBS reacts slowly and at very early ages (<7d), some authors [13,50,51] have reported limited reaction, suggesting participation through the physical mechanisms of filler and dilution effects [25], which in turn enhance clinker hydration [11]. However, analysis of simulated and cement pore solutions [12,52] suggests a chemical contribution but this has not been quantified nor the effect of secondary anions that are commonly found in composite cements (sulphates, carbonates and their combinations) elucidated. The simplified systems of calcium hydroxide and GGBS provide insight into the synergy between limestone and calcium sulphate in modifying early age and long-term hydration of GGBS in composite cements. This section is focused upon clarifying consumption of the anionic species and how they in turn affect GGBS hydration.

Reaction rates of anhydrite and limestone

Anhydrite, limestone, or their combination influenced the reaction kinetics of the GGBS-calcium hydroxide systems differently. Their presence resulted in greater heat evolution (Fig. 3) compared to the control GGBS and calcium hydroxide mix. TGA and micro-analysis (Figs. 4–8) confirmed continued formation of silicate and aluminate bearing phase assemblages over time. In these systems, GGBS was the only source of silicon and aluminium and hence precipitation of the silicon and aluminium bearing phase assemblages are indicative of GGBS dissolution. As shown in Fig. 10(a and b), AFm and ettringite contents differed and as did their evolution over time, indicative of differences in the dissolution kinetics of the constituents. Elucidating the consumption of anhydrite and limestone in these systems is critical for understanding how they affected the hydration of GGBS (discussed in the next section).

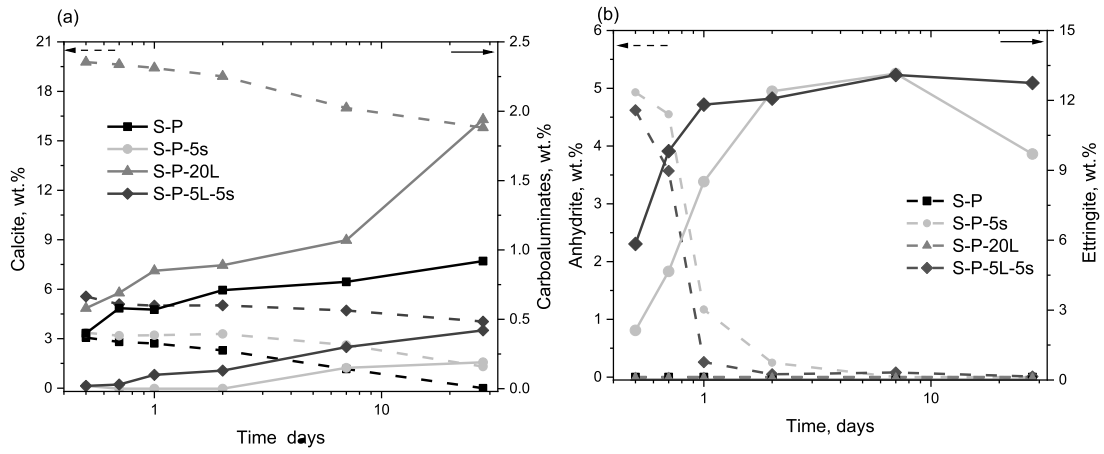

Fig. 10. Quantitative XRD analysis showing (a) consumption of calcite (dashed lines) and formation of hemicarboaluminate (solid lines) and (b) consumption of anhydrite (dashed lines) and ettringite formation (solid lines).
Note: The GGBS and calcium hydroxide used in this investigation contained 2.4 and 1.2% calcite respectively.

Combined limestone and anhydrite addition modified their respective consumption and the resulting hydrates compared to the mixes that contained only one addition. This is demonstrated in the XRD patterns in Fig. 4 and from the quantitative analysis shown in Fig. 10. Anhydrite retarded limestone dissolution such that, whilst the ~2.4% calcite present in the GGBS fully reacted in the sulphate-free control mix, being incorporated into hemi-carboaluminate, only a small amount was consumed in the mix that contained both anhydrite and limestone. The carboaluminate content in the latter was relatively small even after 28 days of reaction compared to the control. Similarly, in the mix that contained 20% limestone, more calcite reacted, resulting in a significantly higher carboaluminate content. This implies that dissolved carbonates were in part a limiting factor for carboaluminate formation. In the control mix (S-P), these dissolved congruently as the GGBS, but the lack of competitive anions readily led to carboaluminate formation. Conversely, in the presence of limestone, anhydrite consumption was accelerated, leading to faster ettringite formation than in the mix containing only anhydrite. Here, depletion of anhydrite destabilized ettringite and monosulphoaluminate formed as more GGBS reacted. Dissolved carbonates stabilizing ettringite has been extensively reported [35,40,46,47]. However, crystalline hydrotalcite reflections (See Fig. 7) were less distinct in the sulphate-containing mixes, with or without limestone. By virtue of its comparable ionic charge to CO_3^{2-}, SO_4^{2-} should not obstruct hydrotalcite formation [38], but hindered calcite solubility in the presence of sulphates, ostensibly due to the common ion effect, seems to proportionately impede precipitation of hydrotalcite. This in part explains the monosulfoaluminate reflection in the mix without limestone and the greater calcite consumption in the mix without anhydrite.

Effect of sulphate and carbonate on GGBS dissolution

From the calorimetry data (Fig. 3), limestone accelerated the silicate reaction (in this case GGBS), shortening the induction period, and increasing the silicate reaction peak intensity. This effect is consistent with the literature [25,40,52]. However, the rate of reaction at the acceleration stage was lower than the control and the sulphate-containing mixes. This suggests that enhanced reaction due to nucleation as derived from limestone was short-lived and marginally contributed to GGBS reaction during the early stages. Anhydrite, despite not accelerating the onset of GGBS dissolution as noticed in OPC [35], rather increased the reaction rate significantly compared to limestone and similarly enhanced the aluminate reaction. Unlike limestone, the role of anhydrite was not nucleation induced, but seemed to arise from under-saturation. In these systems, calcium availability was not a limiting factor as opposed to the systems in [12,16]. It is plausible that rapid precipitation of ettringite (Figs. 7 and 8) rendered the pore solution undersaturated with respect to aluminium, requiring further dissolution of GGBS to maintain charge balance. This hypothesis is in agreement with the data reported here and elsewhere [14,23].

To evaluate the impact on GGBS hydration, the QXRD/PONKCS method and SEM/IA were used to measure the residual GGBS content from which the degree of hydration was calculated, and the results shown in Fig. 11 together with the residual calcium hydroxide content as calculated from TGA. GGBS reacted in all mixes at early ages such that the degree of reaction after 12 h ranged between 5 and 10%, depending on composition, being greater in the sulphate-containing blends than in the blend with limestone only. Although there were differences in reaction degree up to 1 day, these were small compared to the error associated with the QXRD/PONKCS technique. It must be noted however that accuracy of the QXRD/PONKCS technique can be sensitive to sample preparation and in particular the applied hydration stoppage technique [53,54]. In the mixtures investigated, w/s ratio was maintained at 0.5, and the XRD scans performed on freshly ground samples. This meant the total water in the samples rather than bound water was accounted for in the mass attenuation coefficient calculation, as implemented elsewhere [55]. Consequently, potential errors arising from

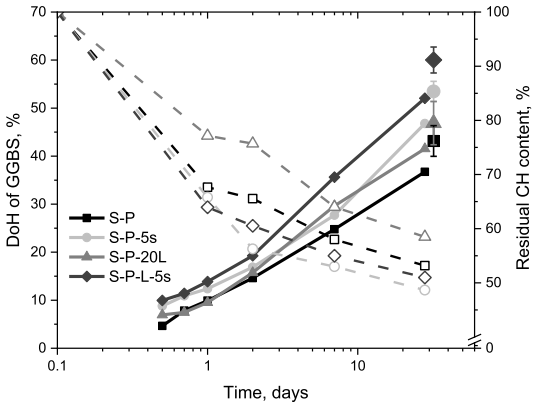

Fig. 11. Degree of hydration of GGBS as measured by the QXRD/PONKCS and SEM/IA methods and the unconsumed calcium hydroxide in the matrix. Note: Solid lines and symbols represent degree of hydration of GGBS and dashed lines and open symbols for residual calcium hydroxide content. SEM/IA was only performed on samples cured for 28 days and error bars of the SEM/IA measurement shown in the figure. The calcium hydroxide content was determined from TGA using the tangent method.

attenuation cannot be responsible for the observed trends.

Anhydrite influenced the reaction degree at the early age more significantly than did limestone, probably due to greater solubility of sulphates than carbonates and resulting undersaturation of aluminium.

The distinct contribution of the composite anhydrite-limestone mix to GGBS hydration became apparent after 1 day. Undersaturation-induced GGBS hydration was comparable in the mixes containing just anhydrite or limestone. The degree of GGBS hydration was greater in the composite anhydrite and limestone mix, but was lowest in the control mix, which contained neither. The trends after 7 days are consistent with the cumulative heat measured in the samples while the trends in degree of hydration after 28 days is consistent between QXRD/PONKCS and SEM/IA. Overestimation in the latter is due to resolution of the SEM/IA technique.

Dominance of calcium in the pore solution has been shown to inhibit GGBS hydration [12,13,21]. In this case, the pore solution was already saturated with calcium hydroxide and more of it remained after 28 days, but GGBS continued to hydrate. This means that retarded GGBS dissolution due to calcium activity is not supported by the data presented here. Instead, a strong dependency on the anionic species in the pore solution is plausible. The fact that GGBS hydration was affected differently by the individual additions and was lowest in the control mix poses important questions over the contribution of the pore solution effects versus space availability. Deductions can be made about the pore solution effect from elemental analysis of the hydrated matrix, assuming equilibrium with the pore solution. In addition to hydrotalcite, and the AFt/AFm assemblages (Figs. 8 and 9), the C-[A]-S-H is the main product following GGBS hydration [19,56–59]. However, the aluminium bearing phase assemblages and their contents affected the latter's incorporation into the C-[A]-S-H. Consequently, these were analysed for each mix after 28 days using SEM/EDX and the results shown in Fig. 12a. Intermixing of other hydrates in the C-[A]-S-H couldn't be ruled out but was minimized by performing EDX analysis at 5000x magnification. The C-[A]-S-H Ca/Si ratios were highest in the sulphate-containing mixes; reducing slightly from 1.47 to 1.44 in the limestone and sulphate-containing mixes. Higher Ca/Si ratios compared to the mixes without sulphate is suggestive of additional calcium emanating from the reaction of anhydrite [19] since less calcium is used to form ettringite (~26.8%) than that contained in anhydrite (~38.3%). Elevated sulphate absorption into the C-[A]-S-H in the sulphate-containing mixes and further in the presence of limestone is noticed in Fig. 12b.

Similarly, less CaO is contained in carboaluminate (~39.7%) than in calcium carbonate (~56%). Therefore, differences in Ca/Si may be associated with dissolved silicate contents and also the higher calcium

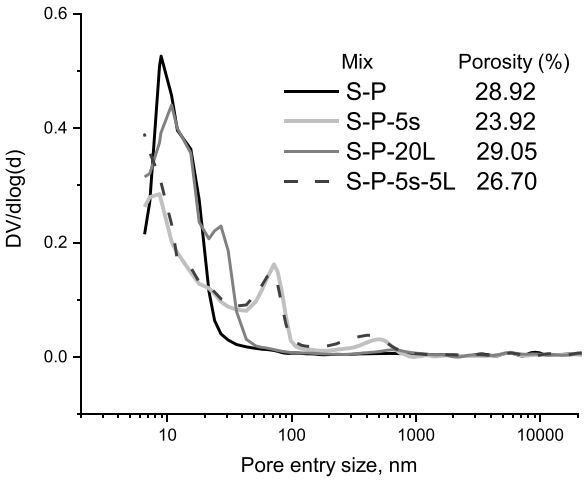

Fig. 12b. Influence of limestone and anhydrite on the pore size distribution and porosity of GGBS-calcium hydroxide mixes.

concentration in AFm phases compared to ettringite [32]. Comparison between the mixes S-P and S-P-20L show slightly higher C-[A]-S-H Ca/Si ratio in the presence of limestone than the mix without. It is worth noting that both mixes contained 20% calcium hydroxide. Therefore, additional calcium from dissolved calcite [25] may also explain the higher Ca/Si ratio.

Additionally, Fig. 12a shows differences in the C-[A]-S-H Al/Si ratios in the different mixes. The Al/Si ratio was reduced significantly when limestone was added. This is because the aluminium was consumed by the formation of carboaluminate phases. In the systems containing sulphates, there was less aluminium consumption due to ettringite having a lower Al content then carboaluminates [32,33].

Implications on the pore structure

Limited availability of capillary pore water has been suggested elsewhere as a possible reason for the retarded hydration of GGBS at later ages [13,25,60]. Analysis of the MIP accessible pores supports this hypothesis. The backscattered scanning electron images in Fig. 7 showed precipitation of hydrates (carboaluminates, hydrotalcite and C-[A]-S-H) around unreacted GGBS particles in the sulphate-free mixes, and the reaction product grew over time. In the sulphate-containing mixes however, ettringite seemed to precipitate away from the

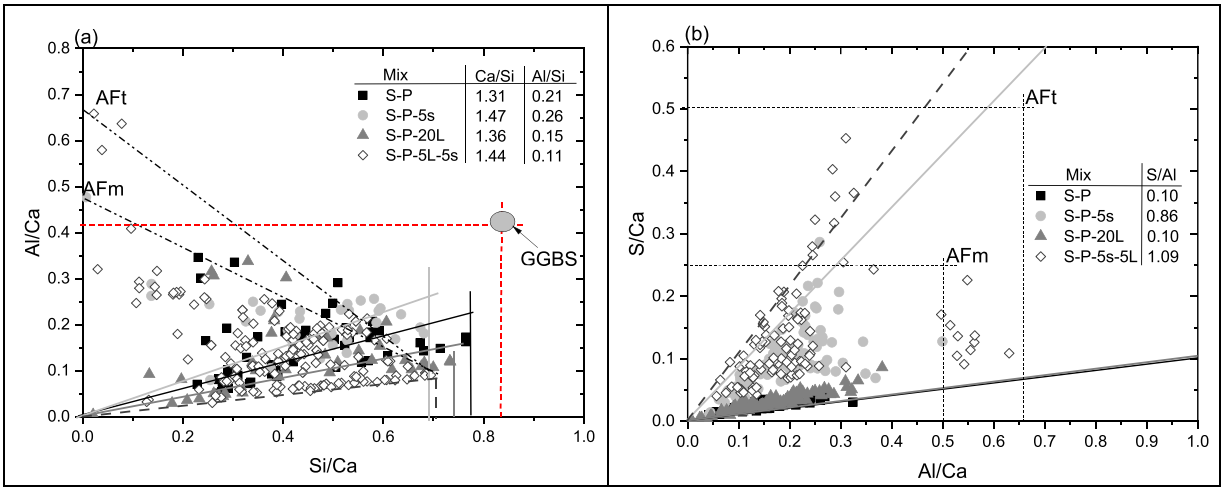

Fig. 12a. Influence of limestone and anhydrite on the (a composition of the C-A-S-H showing the Ca/Si and Al/Si ratios and (b) showing sulphate absorption into the C-A-S-H phase due to anionic species in the GGBS-calcium hydroxide mixes.

reacting GGBS grains (see Fig. 6d and 6h). Consequently, dissolution-controlled reactions would be sustained over longer period in the sulphate-containing mixes as opposed to those in the limestone only or the control samples. Moreover, at medium hydration time (e.g. 28 days) where sufficient hydrates have formed, diffusion of ions would be transported more easily through the needle-like ettringite crystals compared to hydrotalcite or carboaluminates due to the former being less dense [33,34]. This implies that distribution of hydrates around the unreacted GGBS is crucial beyond the dissolution-controlled reaction stage and thus, early precipitation of ettringite plays an important role on medium to long-term reaction of GGBS. An evaluation of the pore size distribution as measured by MIP is shown in Fig. 13. One must recognize that micropores (i.e., < 5 nm) were not probed due to experimental limitation. Notwithstanding, such pores would be dominant in the C-[A]-S-H gel, which should not affect GGBS hydration crucially. Consistent with the phase assemblage evolution (Figs. 7 and 9), the sulphate-containing mixes achieved lower total porosity than the control mix or in the presence of limestone only. The distribution of the pore entry sizes reveals different pore clusters in the binders. Macro-capillary pores were prevalent in the presence of sulphates, likely due to ettringite. Without sulphates, *meso* pores were dominant regardless of whether limestone was present or not. At 0.5 w/b ratio and ~25% bound water in these systems (Fig. 9), excess water existed in these macro-capillary pores to sustain GGBS hydration. On the contrary, without sulphates, although even greater evaporable water was present, these would be located in *meso* pores, possibly remote from reacting GGBS grains. As a result, localized oversaturation around GGBS grains would develop since the dissolved species are not conducted away from the grain to form new hydrates. This could also slow down GGBS dissolution.

Correlation between heat of reaction, bound water and CH consumption

Correlations between the bound water content, consumed calcium hydroxide and heat of reaction up to 7 days were subsequently investigated and the results shown in Fig. 13 (a and b). Additionally, correlations between degree of reaction of GGBS (DoH), bound water and CH consumption are shown in Fig. 13 (c and d). Strong intra-sample correlation was noticed for both the bound water vs. cumulative heat and CH consumed vs. cumulative heat plots (see Fig. 13a and b). For a given sample, the bound water and CH consumption were proportional to the heat of hydration, resulting in a co-efficient of determination (R^2) greater than 0.8 in all cases. However, when different samples were considered at a given age (designated inter-sample) the points were scattered and the correlation as fitted with the red lines (solid at 1d, dashed at 2d and dashed dot at 7d) were only significant for the bound

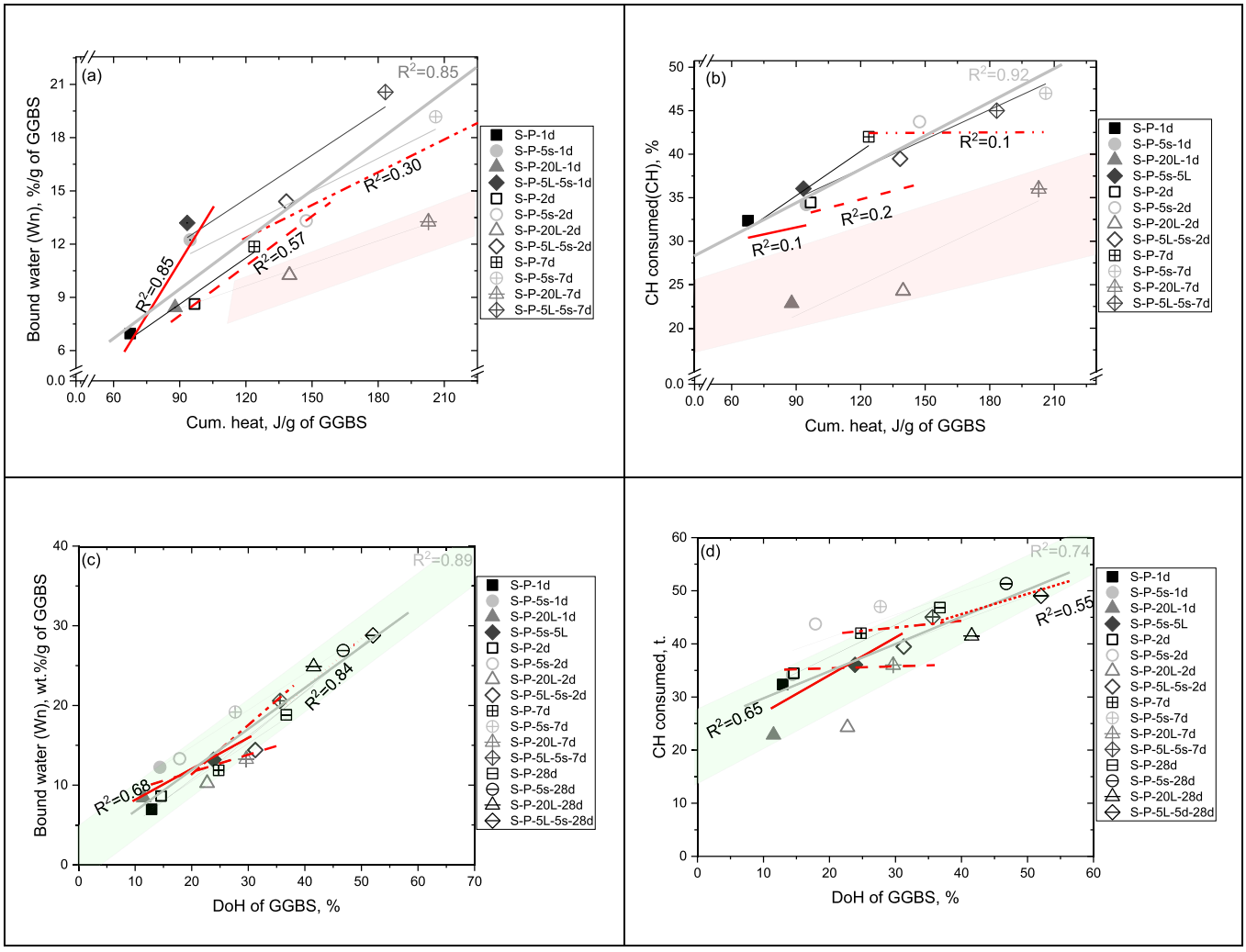

Fig. 13. Correlation test based on: (a) Bound water vs cumulative heat; (b) consumed heat vs cumulative heat measured up to 7d; (c) DoH of Bound water vs GGBS and (d) CH consumed vs GGBS.
Note: Thin lines matching the symbol colour codes indicate intra-sample correlation over the investigated duration; red lines indicate inter-sample correlations where solid:1d, dashed:2d and dashed dot:7d; short dashes (in c and d): 28d. Thick light grey lines are inter-sample correlation.

water versus cumulative heat at 1 day, with the $R^2 = 0.85$. The inter-sample correlations were weaker in the samples older than 1 day (Fig. 13a). Similarly, the stronger intra-sample correlation between the CH consumption versus cumulative heat notwithstanding, the inter-samples' was extremely weak at all ages, see Fig. 13(b), being inconsistent with the R3 test results reported elsewhere [41,43]. Note, the CH/SCM ratio in the R3 test can be greater by a factor of ten plus excess water in the matrix compared to those reported here. Therefore, the observed correlations in this study must be considered in relation to the phase assemblages in the various mixes.

Fig. 13a and 13b show that greater heat of reaction was not always associated with higher CH consumption nor more bound water, as was the case for mix S-P-20L. This accounted for the scatter in the inter-sample correlation plots. Distinct from the plain or sulphate-containing samples, the GGBS-limestone sample (S-P-20L) consumed less CH and water (bound) per unit GGBS reacted (Fig. 13c and d). Both may suggest lower GGBS reactivity and or fewer reaction products. The heat flow (Fig. 2), QXRD and SEM measurements (Fig. 11) do not point to lower degree of reaction of GGBS in the S-P-20L mix. Indeed, the higher CH/GGBS ratio in S-P-20L would be expected to lead to a greater reaction degree than the plain mix as was noticed in Fig. 11 and consistent with the literature [7]. From the DTG endotherms (Fig. 5), the weight of the C-A-S-H phase were comparable between mixes S-P and S-P-20L, although about 6% more was predicted in the S-P mix (Fig. 6), which is due to the 20% reduction in the reactive component. The lower C-A-S-H phase in the S-P-20L can correspondingly reduce bound water. However, on the basis of comparable C-A-S-H content, the phase with higher Ca/Si (Fig. 12), which is S-P-20L in this case would rather incorporate more water into the C-A-S-H phase [61].

It has already been established that mix S-P and S-P-20L differed by the amount of hemicarboaluminate and its conversion to monocarboaluminate (Figs. 8 and 10), the C-A-S-H phase (Fig. 12) and their potential variations with time. Analysis of the stoichiometric compositions of the reaction products coupled with the C-A-S-H phase elemental ratio from SEM/EDX (Fig. 12) can help to explore the role these exert. In Table 4, estimated bound water and calcium (CaO) consumed from the CH into each assemblage are presented. The AFm phases contained higher water content and consumed more CH than the C-A-S-H phase, but the extent clearly depended on the involved phase assemblages. For example, in the S-P-20L mix, monocarboaluminate is stabilized by the additional calcite, which meant reduction in bound water and CH consumption compared to the S-P mix in which hemicarboaluminate and hydrotalcite rather dominated.

Additional to the AFm phases, the C-A-S-H phase in the S-P-20L mix having higher Ca/Si but lower Al/Si ratios also implied lower water content of the C-A-S-H, which is contrary to the expected bound water increase at higher Ca/Si ratio [61]. However, uncertainties in the EDX analysis due to phase intermixing means the slightly lower bound water and corresponding increase in CH consumed from the matrix have to be considered secondary effects and the deviations in the inter-sample correlation attributed to the lower reactive GGBS content.

Table 4
Estimation of the bound water and CaO consumed from CH per phase assemblage in the investigated mixes.

Phase	Phase composition	Wn, %/phase	CaO from CH, %/phase
Ht	$Mg_3Al(OH)_8(CO_3)_{0.5}(H_2O)_{2.5} + 4H^+ = AlO_2^- + 0.5CO_3^{2-} + 3Mg^{2+} + 8.5H_2O3(24.3) +163+0.5(60) +2.5(18) + 4 = 8.5(18)$	48.6	–
Hc	$(CaO)_{3.5}.(CaCO_3)_{0.5}.Al_2O_3.(H_2O)_{10.5} + 5H^+ = 2AlO_2^- + 0.5CO_3^{2-} + 4Ca^{2+} + 13H_2O3.5(56) + 0.5(100) +101.96 + 10.5(18) + 5\ 13(18)$	43.2	36.1
Mc	$(CaO)_3(CaCO_3)Al_2O_3(H_2O)_{11} + 4H^+ = 2AlO_2^- + CO_3^{2-} + 4Ca^{2+} + 13H_2O3(56) + 100 + 101.96 + 11(18) + 4\ 13(18)$	40.9	29.4
AFt	$(CaO)_3(CaSO_4)_3(Al_2O_3).(H_2O)_{30} + 4H^+ = 2AlO_2^- - + 6Ca^{2+} + 3S\|6\|O_4^{2-} + 32H_2O3 (56) + 3(136) + 101.96 + 32(18) + 4\ 32(18)$	47.1	13.7
GGBS*	$Ca_{1.18}SiMg_{0.2}Al_{0.38}$	–	–
C-A-S-H (Ca/Si= 1.31)	$(CaO)_{1.31}(Al_2O_3)_{0.21}(SiO2) : 1.625H_2O + 3.88H^+ = 1.31Ca^{2+} + 0.21Al^{3+} + H_4SiO_4 + 1.565H_2O1.31(56) + 0.21(101.96)+60 + 1.65 (18) + 3.8\ 1.565(18)$	15.1	3.9
C-A-S-H (Ca/Si= 1.36)	$(CaO)_{1.36}(Al_2O_3)_{0.15}(SiO2) : 1.625H_2O + 3.62H^+ = 1.36Ca^{2+} + 0.15Al^{3+} + H_4SiO_4 + 1.435H_2O1.31(56) + 0.21(101.96)+60 + 1.65 (18) + 3.8\ 1.435(18)$	14	5.5
C-A-S-H (Ca/Si= 1.47)	$(CaO)_{1.47}(Al_2O_3)_{0.26}(SiO2) : 1.625H_2O + 4.5H^+ = 1.47Ca^{2+} + 0.26Al^{3+} + H_4SiO_4 + 1.875H_2O1.47(56) +0.26(101.96) + 60 + 1.625(18) + 4.5\ 1.875(18)$	16.7	8.1
C-A-S-H (Ca/Si= 1.44)	$(CaO)_{1.44}(Al_2O_3)_{0.11}(SiO2) : 1.625H_2O + 3.54H^+ = 1.44Ca^{2+} + 0.11Al^{3+} + H_4SiO_4 + 1.395H_2O1.44(56) +0.11(101.96) + 60 + 1.625(18) + 3.54\ 1.395(18)$	13.6	7.9

sulphate, which can limit inter-sample comparisons between bound water and CH consumption with calorimetry and degree of hydration measurements.

The interplay between sulphates and calcium carbonates, noted from the calorimetry reflected also on kinetics of GGBS, anhydrite and limestone dissolution on the one hand and the microstructure. A honeycomb microstructure was seen in the sulphate mixes, and much denser in the mixes without sulphate. Elemental analysis of the hydration products revealed that the sulphate-containing samples attained greater degree of GGBS hydration and led to C-A-S-H with a higher calcium to silicate ratio. Consequently, calcium activity did not inhibit GGBS hydration as suggested in the literature but a combination of anionic species (at early age) and macro-capillary pore space did. This is new insight regarding the factors controlling reactivity of GGBS in limestone ternary cements.

In summary, this work has demonstrated that aluminium uptake into the C-S-H, ettringite, and AFm phases including carboaluminates, monosulphoaluminate, and hydrotalcite plays an important role at the dissolution-controlled reaction stage in composite cements. Distribution of ettringite promotes macro-capillary pores, which is favourable for GGBS hydration. Optimization of the sulphate-limestone contents is thus imperative in achieving the balance between the pore solution and macro-capillary effect for maximizing SCM reactivity.

Conclusions

Hydration of GGBSGGBS in simplified systems comprising calcium hydroxide, carbonates, sulphates or their combination has been studied using a multi-technique approach with a view to clarify the interplay between different anionic species in composite cements. There was moderate acceleration of GGBS dissolution in the presence of carbonates with significant acceleration of the precipitation of aluminate-bearing hydration products in the presence of sulphates. In these simplified systems, formation of aluminium- and silicate-bearing hydrates at such an early stage confirm GGBS reaction. Hydrates comparable to those formed in composite cements were noticed, increasing with time and consuming calcium hydroxide. The extent of calcium hydroxide consumption and the bound water were strongly affected by carbonates and

Declaration of Competing Interest

The authors have no competing interests to declare.

Data availability

Data will be made available on request.

Supplementary materials

Supplementary material associated with this article can be found, in the online version, at doi:10.1016/j.cement.2023.100085.

References

[1] J.I. Escalante, et al., Reactivity of blast-furnace slag in Portland cement blends hydrated under different conditions, Cem. Concr. Res. 31 (10) (2001) 1403–1409.
[2] B. Lothenbach, K. Scrivener, R.D. Hooton, Supplementary cementitious materials, Cem. Concr. Res. 41 (12) (2011) 1244–1256.
[3] K. Scrivener, et al., TC 238-SCM: hydration and microstructure of concrete with SCMs, Mater. Struct. 48 (4) (2015) 835–862.
[4] L. Opoczky, Grinding technical questions of producing composite cements, Int. J. Miner. Process 44-45 (1996) 395–404.
[5] S. Adu-Amankwah, S.A. Bernal Lopez, L. Black, Influence of component fineness on hydration and strength development in ternary slag-limestone cements, RILEM Tech. Lett. 4 (0) (2019) 81–88.
[6] M. Öner, K. Erdoğdu, A. Günlü, Effect of components fineness on strength of blast furnace slag cement, Cem. Concr. Res. 33 (4) (2003) 463–469.
[7] J.J. Biernacki, et al., Kinetics of slag hydration in the presence of calcium hydroxide, J. Am. Ceram. Soc. 85 (9) (2002) 2261–2267.
[8] T. Saeki, P.J.M. Monteiro, A model to predict the amount of calcium hydroxide in concrete containing mineral admixtures, Cem. Concr. Res. 35 (10) (2005) 1914–1921.
[9] S.C. Pal, A. Mukherjee, S.R. Pathak, Investigation of hydraulic activity of ground granulated blast furnace slag in concrete, Cem. Concr. Res. 33 (9) (2003) 1481–1486.
[10] M.B. Haha, et al., Influence of slag chemistry on the hydration of alkali-activated blast-furnace slag — part I: effect of MgO, Cem. Concr. Res. 41 (9) (2011) 955–963.
[11] J. Skibsted, R. Snellings, Reactivity of supplementary cementitious materials (SCMs) in cement blends, Cem. Concr. Res. 124 (2019), 105799.
[12] R. Snellings, Solution-controlled dissolution of supplementary cementitious material glasses at pH 13: the effect of solution composition on glass dissolution rates, J. Am. Ceram Soc. 96 (8) (2013) 2467–2475.
[13] Y. Briki, et al., Factors affecting the reactivity of slag at early and late ages, Cem. Concr. Res. 150 (2021), 106604.
[14] M. Whittaker, et al., The role of the alumina content of slag, plus the presence of additional sulfate on the hydration and microstructure of Portland cement-slag blends, Cem. Concr. Res. 66 (2014) 91–101.
[15] O.R. Ogirigbo, L. Black, Influence of slag composition and temperature on the hydration and microstructure of slag blended cements, Constr. Build. Mater. 126 (2016) 496–507.
[16] M. Ben Haha, et al., Influence of activator type on hydration kinetics, hydrate assemblage and microstructural development of alkali activated blast-furnace slags, Cem. Concr. Res. 41 (3) (2011) 301–310.
[17] S. Kucharczyk, J. Deja, M. Zajac, Effect of slag reactivity influenced by alumina content on hydration of composite cements, J. Adv. Concr. Technol. 14 (9) (2016) 535–547.
[18] S. Kucharczyk, et al., Structure and reactivity of synthetic CaO-Al_2O_3-SiO_2 glasses, Cem. Concr. Res. 120 (2019) 77–91.
[19] D.K. Dutta, P.C. Borthakur, Activation of low lime high alumina granulated blast furnace slag by anhydrite, Cem. Concr. Res. 20 (5) (1990) 711–722.
[20] E.H. Oelkers, General kinetic description of multioxide silicate mineral and glass dissolution, Geochim. Cosmochim. Acta 65 (21) (2001) 3703–3719.
[21] J. Fu, et al., Mechanisms of enhancement in early hydration by sodium sulfate in a slag-cement blend – insights from pore solution chemistry, Cem. Concr. Res. 135 (2020), 106110.
[22] G.J. Stockmann, et al., The role of silicate surfaces on calcite precipitation kinetics, Geochim. Cosmochim. Acta 135 (2014) 231–250.
[23] P. Suraneni, M. Palacios, R.J. Flatt, New insights into the hydration of slag in alkaline media using a micro-reactor approach, Cem. Concr. Res. 79 (2016) 209–216.
[24] W. Hinrichs, I. Odler, Investigation of the hydration of Portland blastfurnace slag cement: hydration kinetics, Adv. Cem. Res. 2 (5) (1989) 9–13.
[25] E. Berodier, K. Scrivener, Understanding the filler effect on the nucleation and growth of C-S-H, J. Am. Ceram. Soc. 97 (12) (2014) 3764–3773.
[26] K.L. Scrivener, A. Nonat, Hydration of cementitious materials, present and future, Cem. Concr. Res. 41 (7) (2011) 651–665.
[27] S.L. Brantley, Reaction kinetics of primary rock-forming minerals under ambient conditions, in: Treatise on Geochemistry 5, Editor: J.I. Drever, 2003, p. 605.
[28] E.H. Oelkers, J. Schott, J.L. Devidal, The effect of aluminum, pH, and chemical affinity on the rates of aluminosilicate dissolution reactions, Geochim. Cosmochim. Acta 58 (9) (1994) 2011–2024.
[29] T. Chappex, K.L. Scrivener, The influence of aluminium on the dissolution of amorphous silica and its relation to alkali silica reaction, Cem. Concr. Res. 42 (12) (2012) 1645–1649.
[30] A. Berg, S.A. Banwart, Carbon dioxide mediated dissolution of Ca-feldspar: implications for silicate weathering, Chem. Geol. 163 (1–4) (2000) 25–42.
[31] S. Adu-Amankwah, et al., Effect of sulfate additions on hydration and performance of ternary slag-limestone composite cements, Constr. Build. Mater. 164 (2018) 451–462.
[32] T. Matschei, B. Lothenbach, F.P. Glasser, The role of calcium carbonate in cement hydration, Cem. Concr. Res. 37 (4) (2007) 551–558.
[33] T. Matschei, B. Lothenbach, F.P. Glasser, The AFm phase in Portland cement, Cem. Concr. Res. 37 (2) (2007) 118–130.
[34] M. Balonis, F.P. Glasser, The density of cement phases, Cem. Concr. Res. 39 (9) (2009) 733–739.
[35] M. Zajac, et al., Influence of limestone and anhydrite on the hydration of Portland cements, Cem. Concr. Compos. 46 (0) (2014) 99–108.
[36] F. Zunino, K. Scrivener, The influence of the filler effect on the sulfate requirement of blended cements, Cem. Concr. Res. 126 (2019), 105918.
[37] M. Balonis, M. Mędala, F.P. Glasser, Influence of calcium nitrate and nitrite on the constitution of AFm and AFt cement hydrates, Adv. Cem. Res. 23 (3) (2011) 129–143.
[38] S.H.J. Eiby, et al., Competition between chloride and sulphate during the reformation of calcined hydrotalcite, Appl. Clay Sci. 132-133 (2016) 650–659.
[39] V.S. Ramachandran, et al., Handbook of Thermal Analysis of Construction Materials, NOYES Publications, 2002, pp. 72–136.
[40] S. Adu-Amankwah, et al., Influence of limestone on the hydration of ternary slag cements, Cem. Concr. Res. 100 (2017) 96–109.
[41] F. Avet, et al., Development of a new rapid, relevant and reliable (R^3) test method to evaluate the pozzolanic reactivity of calcined kaolinitic clays, Cem. Concr. Res. 85 (2016) 1–11.
[42] S. Blotevogel, et al., Ability of the R3 test to evaluate differences in early age reactivity of 16 industrial ground granulated blast furnace slags (GGBS), Cem. Concr. Res. 130 (2020), 105998.
[43] F. Avet, et al., Report of RILEM TC 267-TRM phase 2: optimization and testing of the robustness of the R3 reactivity tests for supplementary cementitious materials, Mater. Struct. 55 (3) (2022) 92.
[44] D. Herfort, B. Lothenbach, Ternary phase diagrams applied to hydrated cement, in: K. Scrivener, R. Snellings, B. Lothenbach (Eds.), A Practical Guide to Microstructural Analysis of Cementitious Materials, CRC Press, 2016, pp. 485–500.
[45] D. Jansen, et al., The early hydration of Ordinary Portland Cement (OPC): an approach comparing measured heat flow with calculated heat flow from QXRD, Cem. Concr. Res. 42 (1) (2012) 134–138.
[46] K. De Weerdt, et al., Synergy between fly ash and limestone powder in ternary cements, Cem. Concr. Compos. 33 (1) (2011) 30–38.
[47] A. Machner, et al., Limitations of the hydrotalcite formation in Portland composite cement pastes containing dolomite and metakaolin, Cem. Concr. Res. 105 (2018) 1–17.
[48] H.F.W. Taylor, Cement Chemistry, 2nd ed., Thomas Telford, 1997.
[49] W. Chen, H.J.H. Brouwers, The hydration of slag, part 2: reaction models for blended cement, J. Mater Sci. 42 (2) (2007) 444–464.
[50] P.T. Durdziński, et al., Outcomes of the RILEM round robin on degree of reaction of slag and fly ash in blended cements, Mater. Struct. 50 (2) (2017) 135.
[51] I. Pane, W. Hansen, Investigation of blended cement hydration by isothermal calorimetry and thermal analysis, Cem. Concr. Res. 35 (6) (2005) 1155–1164.
[52] A. Schöler, et al., Early hydration of SCM-blended Portland cements: a pore solution and isothermal calorimetry study, Cem. Concr. Res. 93 (2017) 71–82.
[53] S. Adu-Amankwah, et al., Impact of hydration stoppage on quantification of the GGBS content in ternary limestone cements using the PONKCS method, Mater. Struct. 56 (6) (2023) 113.
[54] Adu-Amankwah, S., Black L., and Zajac M., Application of the Rietveld-PONKCS technique for quantitative analysis of cements and pitfalls of hydration stopping methods, Adv. Civil Eng. Mater.. 2022. 11(2).
[55] C. Naber, et al., The PONKCS method applied for time resolved XRD quantification of supplementary cementitious material reactivity in hydrating mixtures with ordinary Portland cement, Constr. Build. Mater. 214 (2019) 449–457.
[56] I.G. Richardson, et al., Location of aluminum in substituted calcium silicate hydrate (C-S-H) gels as determined by ^{29}Si and ^{27}Al NMR and EELS, J. Am. Ceram. Soc. 76 (9) (1993) 2285–2286.
[57] I.G. Richardson, J.G. Cabrera, The nature of C-S-H in model slag-cements, Cem. Concr. Compos. 22 (4) (2000) 259–266.
[58] I.G. Richardson, G.W. Groves, The structure of the calcium silicate hydrate phases present in hardened pastes of white Portland cement/blast-furnace slag blends, J. Mater. Sci. 32 (18) (1997) 4793–4802.
[59] J.M. Richardson, et al., Stoichiometry of slag hydration with calcium hydroxide, J. Am. Ceram Soc. 85 (4) (2002) 947–953.
[60] M. Zajac, et al., Late hydration kinetics: indications from thermodynamic analysis of pore solution data, Cem. Concr. Res. 129 (2020), 105975.
[61] I.G. Richardson, Model structures for C-(A)-S-H(I), Acta Cryst. B 70 (2014) 903–923.